https://doi.org/10.52131/jmps.2021.0202.0016

Journal of Materials and Physical Sciences

Volume 2, Number 2, 2021, Pages 54 - 68

Journal Homepage:
https://journals.internationalrasd.org/index.php/jmps

JOURNAL OF MATERIALS AND PHYSICAL SCIENCES
INTERNATIONAL RESEARCH ASSOCIATION FOR SUSTAINABLE DEVELOPMENT

Role of Tb-Cr Substitution on the Structural and Magnetic Properties of Cobalt Ferrites

Abdul Hameed[1], Muhammad Waqas Khaliq[2*]

[1] Institute of Physics, The Islamia University of Bahawalpur, Bahawalpur-63100, Pakistan
[2] ALBA Synchrotron Light Source, Carrer de la Llum, 2, 26, 08290 Cerdanyola del Vallès, Barcelona, Spain

ARTICLE INFO

Article History:
Received: July 18, 2021
Revised: September 16, 2021
Accepted: December 29, 2021
Available Online: December 31, 2021

Keywords:
Spinel Ferrites
X-Ray Diffraction
Magnetization
Coercive Force
Dielectric Properties

ABSTRACT

The impact of Tb-Cr substitution in cobalt-based ferrites having composition $Co_{1-x}Tb_xFe_{2-y}Cr_yO_4$ (x=0.0-0.1, y=0.0-0.5) prepared by solid state reaction method on structural, magnetic and dielectric parameters was explored. Structural analysis was carried out by X-ray diffraction technique. A variation in lattice parameter (a) was observed as a function of doping. The lattice constant 'a' increases from 8.37 Å to 8.39 Å, whereas crystallite size (D) decreases from 44 nm to 28 nm with Tb-Cr substitution. Unit cell volume was found in the range 586.8 $Å^3$ - 590.6 $Å^3$. X-ray density, bulk density as well as porosity were also affected with the inclusion of Tb-Cr ions. Saturation magnetization and remanence were observed to decrease from 62 emu/g to 51 emu/g and 13.38 emu/g to 8.29 emu/g, respectively with the addition of Tb-Cr contents. The incorporation of Tb-Cr cations caused the decrease in dielectric parameters like dielectric constant as well as dielectric loss.

*Corresponding Author's Email: mkhaliq@cells.es

1. Introduction

Ferrites, magnetic materials, are relatively inexpensive and thermally stable than other magnetic materials. These materials have extensive industrial applications like high-frequency circuits, transformer cores, high-quality filters, and operating devices (Shirsath, Jadhav, Toksha, Patange, & Jadhav, 2011). The field of spinel ferrite is an important class of ferrite family due to its potential applications in different fields such as electronics, modern technology, and electrical and microwave industries. Multilayer chip indicators are unique, essential elements of modern electronics products used in videos cameras, notebook computers, cellular phones, and silver electrodes (Bhandare, Jamadar, Pathan, Chougule, & Shaikh, 2011). The researchers and engineers have investigated that Nano-ferrites show tremendous properties compared to their bulk counterparts. In the nano regime, grain boundaries control physical properties instead of grains (Gadkari, Shinde, & Vasambekar, 2013).

Recently, cobalt ferrites have been extensively focused on their use in electrical and microwave industries, such as reflection coils, antennas, inductors, transformers cores, and nano-metric scales as ultrafine powders (Patange et al., 2011). Though, the uses of ferrites depend on their soft magnetic and hard magnetic nature. Ferrites exhibiting a high coercive field (H_c) are an essential parameter as these materials having significant coercivity can be used in many advanced applications. Cobalt ferrite is considered a hard magnetic material because of its large coercivity and reasonable saturation magnetization, a prerequisite for high-density magnetic recording and data storage devices. Their high coercivity value results from the high anisotropy of the Co^{2+} ions because of its significant spin-orbit coupling (Mallapur et al., 2009). Electrical and magnetic characteristics of ferrites

can be tailored by doping the transition metals (Ni, Co, Zn, Cd, etc.) as well as the rare earth elements (Gd, Dy, Tb, etc.) synthesized via various techniques (Ahmed, Afify, El Zawawia, & Azab, 2012; Batoo, Kumar, Lee, & Alimuddin, 2009; Zhao et al., 2006). The distribution of cations at octahedral (B) and tetrahedral (A) sites plays a chief role in controlling the structural, electric, dielectric, and magnetic behavior (G. Kumar et al., 2013).

The rare earth cations have unpaired 4f electrons with ionic radii larger than Fe cation when substituted in spinel ferrite lattice, ensuring structural, magnetic, and electrical properties (Asif Iqbal et al., 2014). S. G Kakade et al. synthesized the Er^{3+} substituted cobalt ferrites and studied that structural, electrical, magnetic, and dielectric parameters were changed and exhibited significant changes with doping the rare earth metals. The optimized electric resistivity shows that the prepared samples are applicable for decreasing eddy current losses at large frequency regions and can be suitable for multilayer chip inductor (MLCI) devices (Kakade, Kambale, Kolekar, & Ramana, 2016). H-z Duan et al. investigated the influence of rare earth cation on absorbing and magnetic properties of Ce doped Ni-Co hollow spheres nanoparticles synthesized via hydrothermal method (Duan, Zhou, Cheng, Chen, & Li, 2017).

In recent work, we explored the influence of Tb-Cr doping for Fe-Co in cobalt-based ferrites by the standard ceramic method. The cobalt-based ferrites have been explored for their outstanding uses in magnetic recording media and EM attenuation. The central theme of this work is to elucidate the changes in structural parameters, absorption bands, and magnetic as well dielectric properties with doping of transition (Cr) and rare-earth element (Tb). The optimized results of this research are discussed here in detail.

2. Experimental Methods

Cobalt ferrite and Tb-Cr substituted cobalt ferrites were fabricated by the standard ceramic method. Analytical reagents were used to prepare Tb and Cr doped cobalt spinel ferrites with composition $Co_{1-x}Tb_xFe_{2-y}Cr_yO_4$ (x = 0.0-0.1, y=0.0-0.5) using starting materials Fe_2O_3 (Sigma-Aldrich 99.9 %), CoO (Sigma-Aldrich 99.9 %), Tb_4O_7 (Sigma-Aldrich 99.9 %) and Cr_2O_3 (Sigma-Aldrich 99.9 %). These materials were combined in a stoichiometric ratio to prepare the required compositions. The dried residues were then ground for 4 hours using a pestle and mortar to obtain the fine powders. The ground powders were then converted into pellets at a pressure of (~35 KN) for 5 minutes by a Paul-Otto Weber hydraulic press. After that, the samples were firstly sintered at 650 °C for 24 hours and finally sintered at 825 °C for eight hours, followed by air quenching. Differential thermal analysis and thermogravimetric analysis of un-sintered powder were carried out to investigate the sintering temperatures by the thermal analyzer instrument model; Mettler Toledo GC 200), having a heating rate of 10 ºC/min. X-ray diffraction statistics data were collected using Bruker D8-ADVANCED X-ray diffractometer with Cu-Kα radiation (λ=1.54178 Å). Magnetization measurements under an applied magnetic field of ±1T were carried out at room temperature using a quantum design vibrating sample magnetometer (VSM: Model 6000). Dielectric parameters were examined for a frequency range 1MHz to 3GHz using the two probe method.

3. Results and Discussion

3.1. TGA/DTA Analysis

Figure 1 shows the thermogravimetric (TGA), differential gravimetric (DTA), and differential scanning calorimetric (DSC) studies for un-annealed $Co_{0.96}Tb_{0.04}Fe_{1.8}Cr_{0.2}O_4$ ferrite sample. TGA curve depicts that the entire weight loss of material was 19.4 % which was split into four portions. The first loss was 6.24 % at 82 °C, followed by a second loss of 3.16 % at 158.7 °C because of water evaporation. In the third part, 6.9 % weight loss was observed at 262 °C because of the decomposition of another phase before the development of spinel ferrite (Mahmood et al., 2013).

In the last part, weight loss was 2.1% from 262 to 950 °C because of the transition of metal oxides into ferrite materials. This temperature is the annealing temperature [14]. Further, no additional weight loss after 950°C was seen, which proves the complete

breakdown of complexes and shows the completion of phase formation.(Farhadi & Rashidi, 2010).

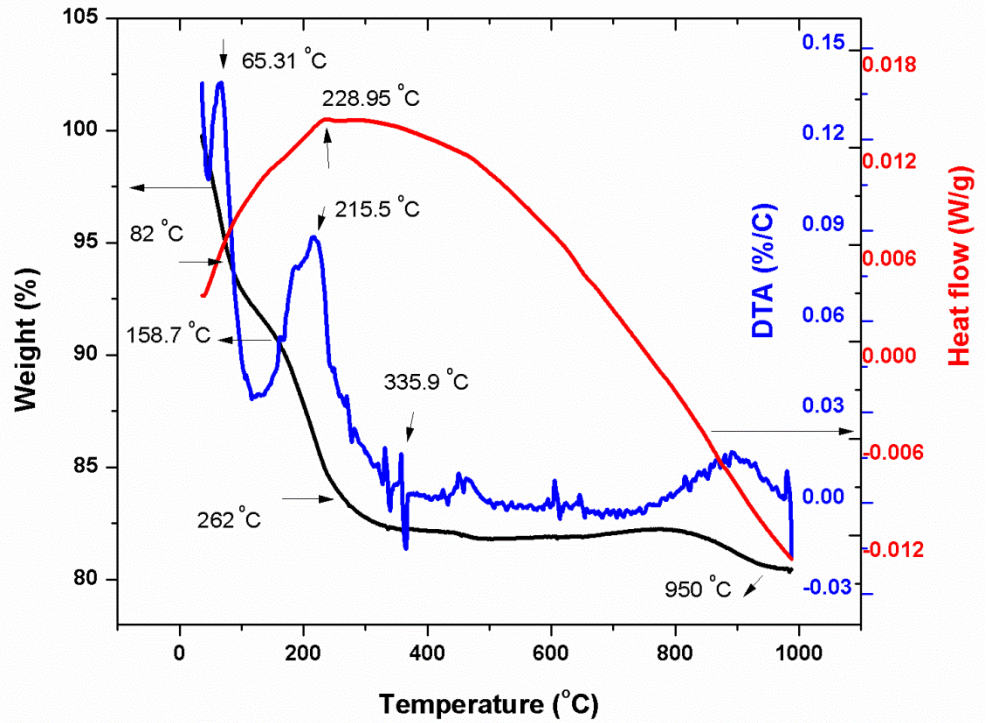

Figure 1: TGA, DTA, DSC curves for as-prepared $Co_{0.96}Tb_{0.04}Fe_{1.8}Cr_{0.2}O_4$ sample

DTA analysis describes the decomposition rate of material. The amount of the reacting substances can be measured through the area of the peak. Endothermic peaks describe phase transition, dehydration, and reduction, while exothermic peaks describe the crystallization and oxidation processes.

The differential scanning calorimetry (DSC) curve of the sample is also shown in Figure 1. In the DTA curve, peaks appeared at 65.31 °C, and 215.5 °C designate the breakdown of anions, whereas a sharp peak at 356 °C depicts the breakdown of metallic complexes. The peak at 228.95 °C describes the exothermic behavior due to the heat evolved during the crystallization of ferrite material.

3.2. Structural Analysis

Figure 2 shows the XRD spectra of terbium and chromium co-doped cobalt ferrites with composition $Co_{01-x}Tb_xFe_{2-y}Cr_yO_4$ (x=0-0.1, y=0.1-0.5).The XRD spectra of entire samples reveal the XRD peaks, which are indexed as (111), (220), (311), (222), (400), (422), (511), and (440) reflections (Muhammad Azhar Khan et al., 2015; Mukhtar et al., 2015). These XRD peaks are the characteristics planes of single-phase cubic spinel structure. The addition of Tb and Cr in the cobalt ferrite exhibits the presence of the $TbFeO_3$ residual phase (*). This peak is observed at an angle of 33. 47° and is found as (322) plane of $TbFeO_3$ orthorhombic phase confirmed through ICDD # 88-0144. The Tb-Cr co-doped cobalt soft ferrites reveal the secondary phase peak, and its intensity gradually increases with the incorporation of dopants. It is also observed that the incorporation of larger radii rare earth cations increases the lattice constant due to the formation of the secondary phase (M. Azhar Khan et al., 2009). The crystallite size of all prepared samples was calculated by Scherrer's formula given as (Iqbal, Ahmad, Meydan, & Nlebedim, 2012).

$$D = \frac{0.9\lambda}{\beta \cos\theta} \quad (1)$$

D shows crystallite size, β shows full width at half maximum (FWHM), λ is X-ray's wavelength, and θ shows diffraction angle. The structural parameters such as lattice constant, cell volume, X-ray density, bulk density, and crystallite size were evaluated from the recorded data of XRD. All these parameters are listed in table 1. Crystallite size exhibits

a non-linear behavior with the increasing contents of Tb and Cr in cobalt ferrite. The decrease in crystallite size has also been reported in the literature by including rare earth cations (Rezlescu, Rezlescu, Pasnicu, & Craus, 1994). The lattice constant increases from 8.372 Å to 8.39 Å with the increase of Tb^{3+} and Cr^{3+} concentration in the spinel lattice of cobalt ferrites.

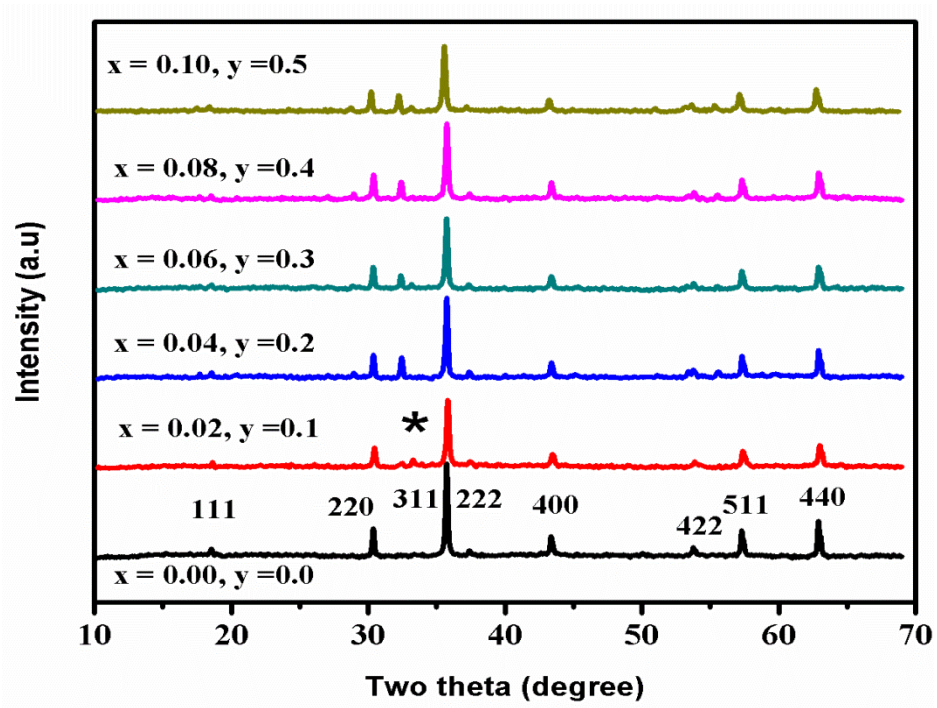

Figure 2: XRD patterns of $Co_{1-x}Tb_xFe_{2-y}Cr_yO_4$ (x = 0.0- 0.10 and y = 0.0- 0.5) ferrites

The cell volume was also increased from 586 $(Å)^3$ to 590 $(Å)^3$. The slight increase in the lattice constant is attributed to the larger ionic radius of Tb^{3+} (0.93 Å) than Co^{2+} (0.74 Å) and smaller ionic radius of Cr^{3+} (0.63 Å) as compared to Fe^{3+} (0.67 Å) (B. Cheng, 2006; John Berchmans, Kalai Selvan, Selva Kumar, & Augustin, 2004). The replacement of smaller cations (Co) with the larger cations (Tb) justified the increase in lattice constant. The bulk densities of all samples were observed to be smaller than X-ray densities, which revealed the presence of pores in these soft ferrites obtained in the preparation or sintering of the ferrite samples. The value of X-ray density increases from 4.79 to 5.09 g/cm^3 with an increasing amount of dopants. It is also obvious from Table 1 that bulk density increases from 3.68 to 3.93 g/cm^3 with the increase of dopants content, and it might be because the Tb ion has a higher atomic weight than the Co cation. The porosity varies from 24.6 to 22.8 %. Similar results were reported in the literature for rare earth substituted cobalt spinel ferrites (Dascalu, Popescu, Feder, & Caltun, 2013; Tahar et al., 2008).

Table 1
Crystallite size (D), Lattice constant (a), Cell volume (V_{cell}), X-ray density (ρ_x), Bulk density (ρ_b), and Porosity (P %) of $Co_{1-x}Tb_xFe_{2-y}Cr_yO_4$ (x = 0.0-0.1, y=0.0-0.5) nano-ferrites

Composition	D (nm)	a (Å)	V_{cell} ($Å^3$)	ρ_x (gm/cm^3)	ρ_b (gm/cm^3)	P (%)
x=0.00, y=0.0	44	8.372	586.8	4.79	3.68	23
x=0.02, y=0.1	43	8.374	587.2	4.86	3.72	23.5
x=0.04, y=0.2	39	8.377	587.8	4.97	3.75	24.5
x=0.06, y=0.3	41	8.382	588.9	5.01	3.78	24.6
x=0.08, y=0.4	32	8.386	589.7	5.06	3.84	24.1
x=0.10, y=0.5	28	8.390	590.6	5.09	3.93	22.8

3.3. Magnetic Properties

M–H loops of pure and Tb-Cr co-doped cobalt ferrites were obtained up to an applied magnetic field of 10 kOe and are exhibited in figures 3a to 3f. Magnetic parameters, i.e.,

coercivity (H_c), saturation magnetization (M_s), and remanence (M_r), were taken out from these loops and are tabulated in table 2. The M_s can also be calculated using the law of approach to saturation (Grossinger, 1981). All the fitted curves of saturation magnetization are calculated using this law at 300 K are shown in figures 4(a-f). All samples revealed high M_s values while coercivity (H_c) values were relatively low, indicating that all the materials showed strong magnetism (Ozkaya et al., 2009). Coercivity values range from a few hundred oersteds for entire materials, and these elucidate the intrinsic behavior of soft ferrites. It was noticed that co-doping of Tb and Cr in Co soft ferrites substantially lowers the coercivity. This decrement in coercivity was attributed to the decrease of the magneto-crystalline anisotropy of Co ferrite; as the concentration of Co decreases that has a high value of magneto-crystalline anisotropy from other cations present in these materials (Kambale, Song, Won, Lee, & Hur, 2012; Ren & Xu, 2014; Sodaee, Ghasemi, Paimozd, Paesano Jr, & Morisako, 2013).

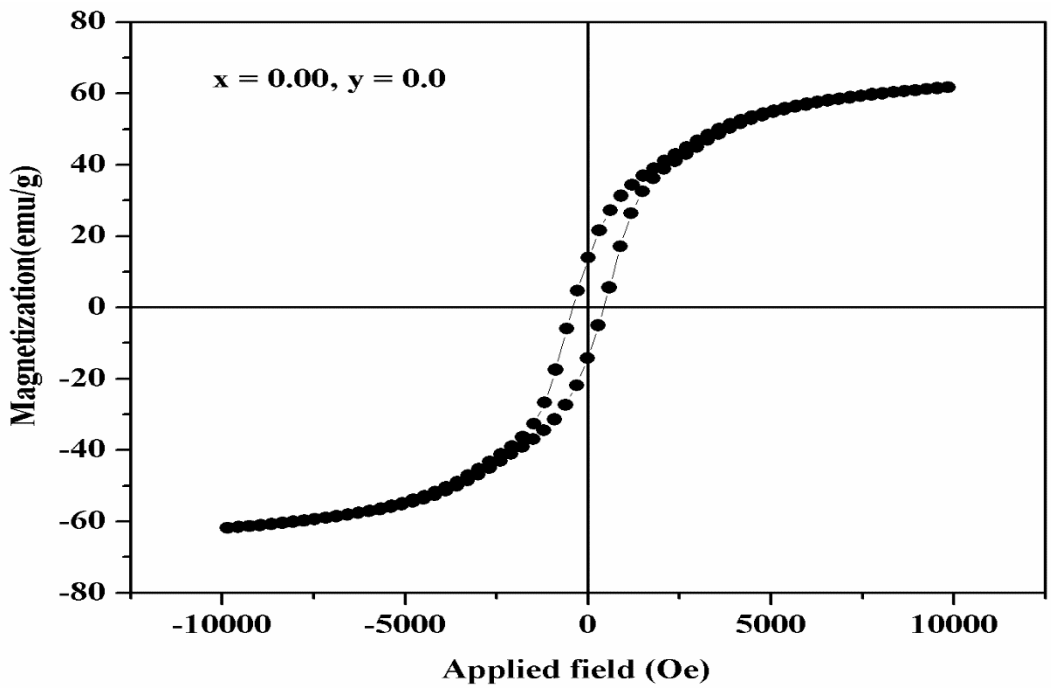

Figure 3a: M-H loop of $CoFe_2O_4$ ferrite

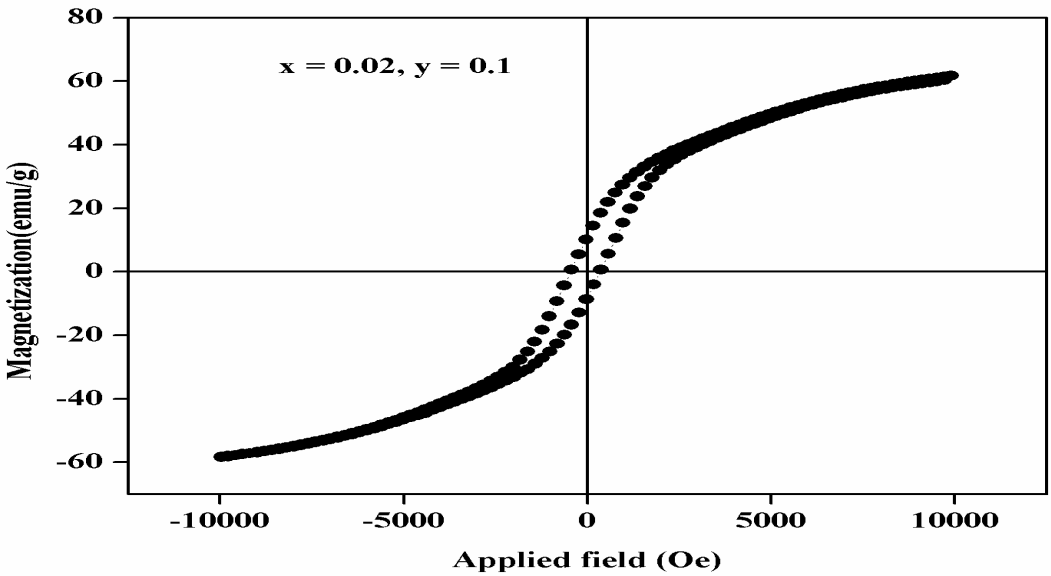

Figure 3b: M-H loop of $Co_{0.98}Tb_{0.02}Fe_{1.9}Cr_{0.1}O_4$ ferrite

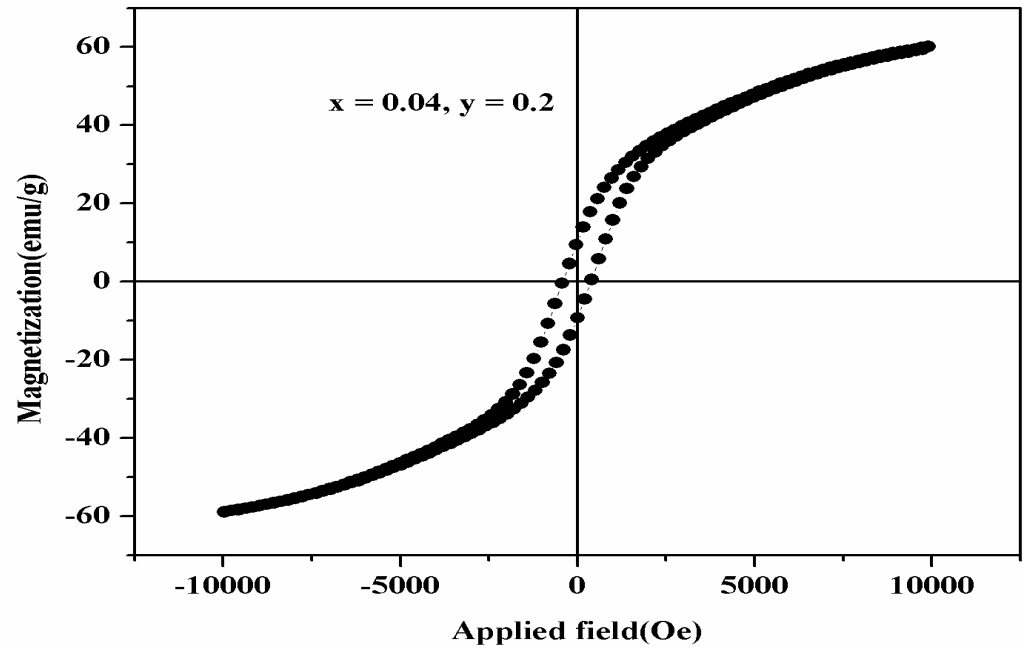

Figure 3c: M-H loop of $Co_{0.96}Tb_{0.04}Fe_{1.8}Cr_{0.2}O_4$ ferrite

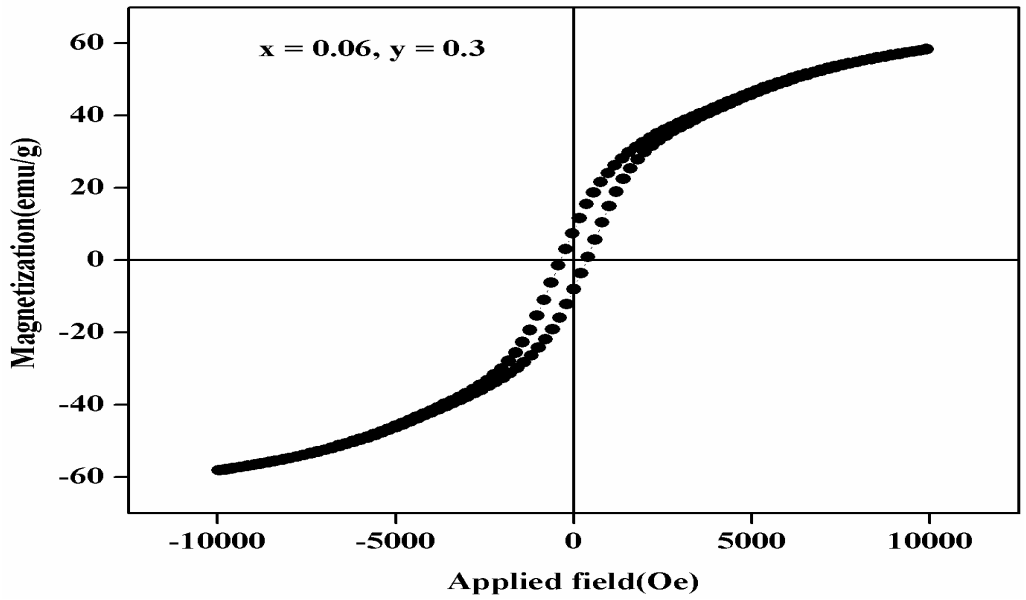

Figure 3d: M-H loop of $Co_{0.94}Tb_{0.06}Fe_{1.7}Cr_{0.3}O_4$ ferrite

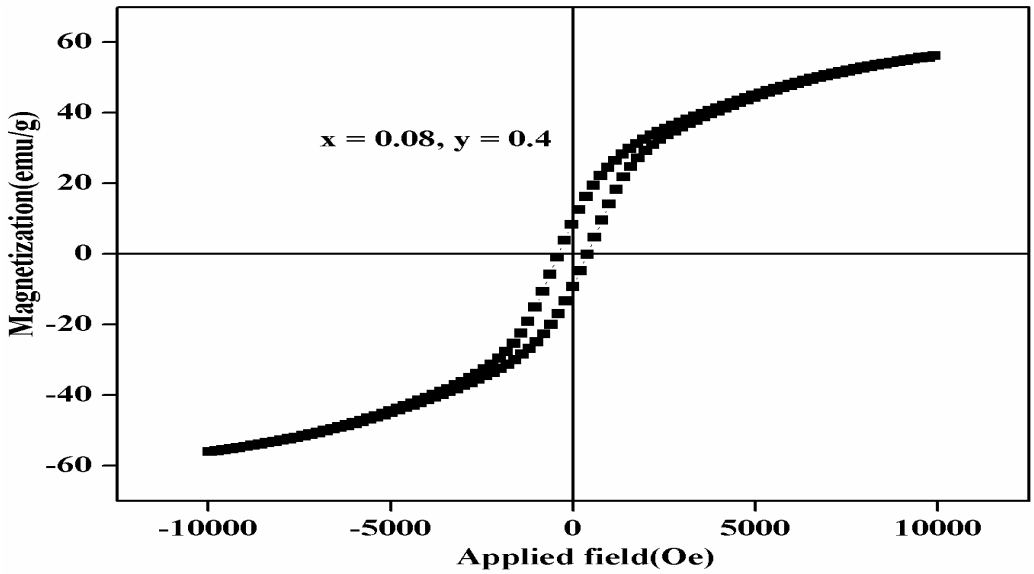

Figure 3e: M-H loop of $Co_{0.92}Tb_{0.08}Fe_{1.6}Cr_{0.4}O_4$ ferrites

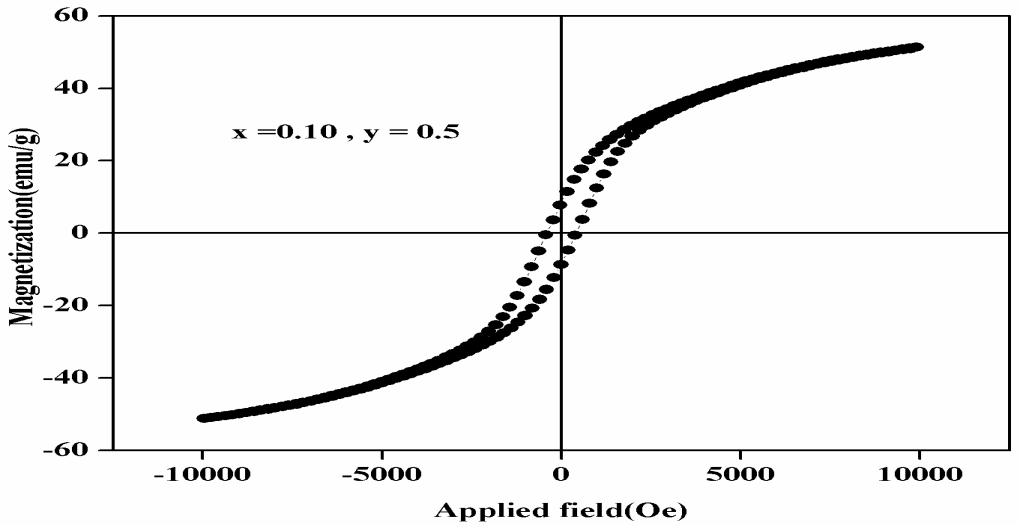

Figure 3f: M-H loop of $Co_{0.90}Tb_{0.10}Fe_{1.5}Cr_{0.5}O_4$ ferrite

The coercive force can be co-related with crystallite size. The larger crystallites provide minimum pinning of domain walls due to the smaller volume fraction of the grain boundaries. It was found that crystallite size exhibits non-linear behavior by increasing doping concentration. Similarly, coercivity first decreases from 425 Oe to 364 Oe, and later it increases for higher dopants concentration. The M_s reduces from 62 to 51 emu/g by increasing the dopants concentration. The decrement in the M_s can be associated with exchange interaction among tetrahedral cations (A-sites) and octahedral cations (B-sites). The decrease in the M_s is due to the dilution of magnetization for Tb^{3+} and Cr^{3+} in the B-site (Panneer Muthuselvam & Bhowmik, 2010; Wells & Ramana, 2013). When a small amount of these dopants are introduced in these ferrites, these paramagnetic cations tend to arrive in the B-sublattice (Y. Y. Li, 1974) and substitute ferromagnetic Co cations at B-sites. Hence, the magnetization decreases, resulting in the M_s decreases for all Tb-Cr co-doped ferrites (L. Kumar & Kar, 2012). The remanence reduces from 13.38 to 8.12 emu/g by increasing the contents of dopants. The fitted curves of M_s, acquired from the law of approach to saturation, are calculated at 300 K for all samples and are shown in figures 4a to 4f.

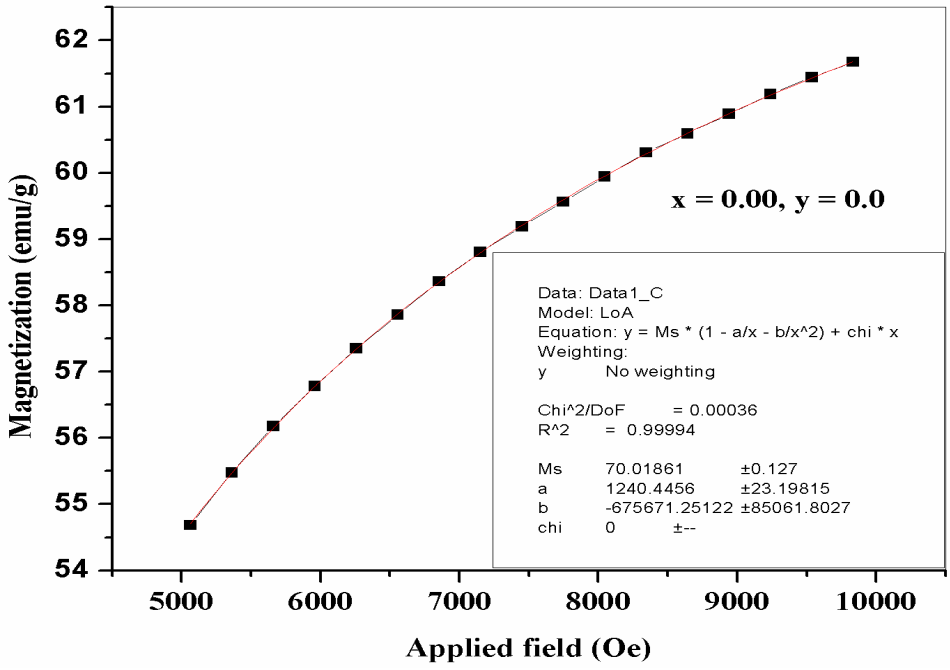

Figure 4a: The fitted curve of M_s at 300 K obtained from the law of approach to saturation for $CoFe_2O_4$ ferrite

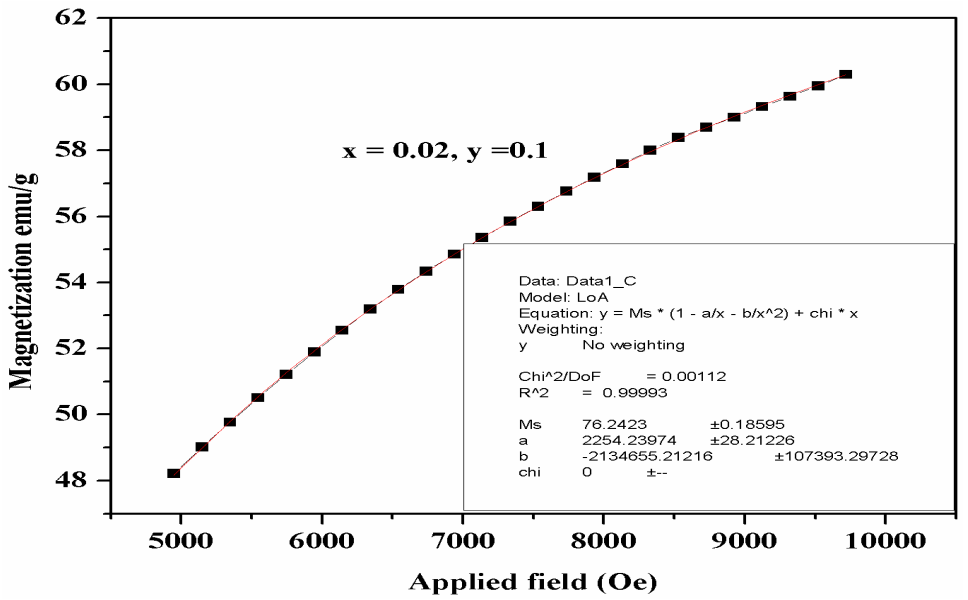

Figure 4b: The fitted curve of M_s at 300 K was obtained from the law of approach to saturation for $Co_{0.98}Tb_{0.02}Fe_{1.9}Cr_{0.1}O_4$ ferrite

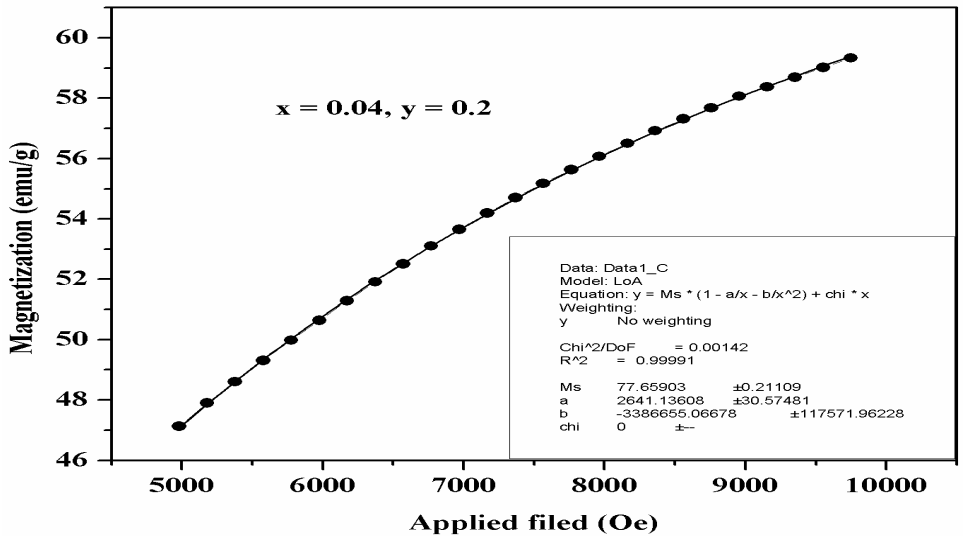

Figure 4c: The fitted curve of M_s at 300 K was obtained from the law of approach to saturation for $Co_{0.96}Tb_{0.04}Fe_{1.8}Cr_{0.2}O_4$ ferrite.

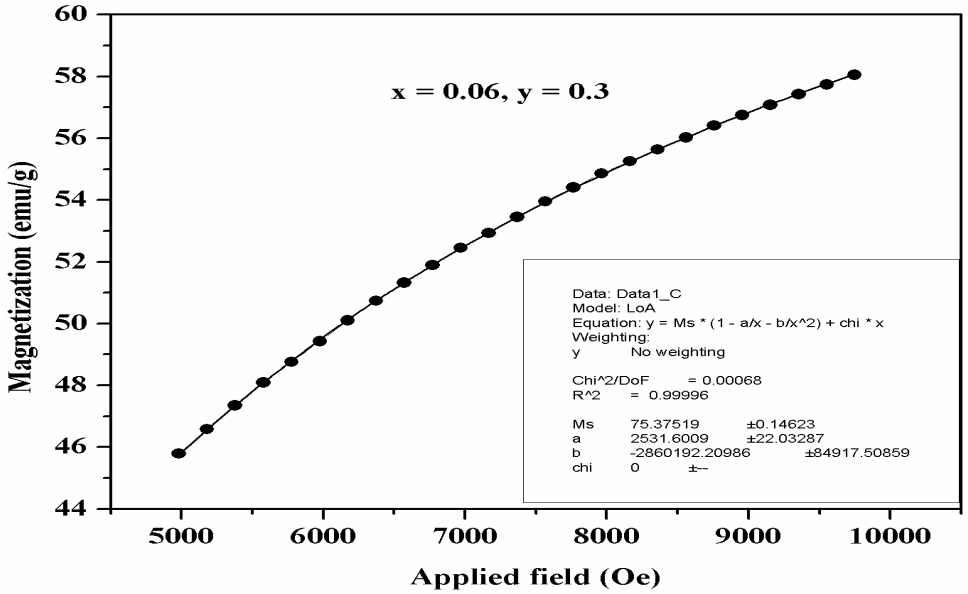

Figure 4d: The fitted curve of M_s at 300 K was obtained from the law of approach to saturation for $Co_{0.94}Tb_{0.06}Fe_{1.7}Cr_{0.3}O_4$ ferrite.

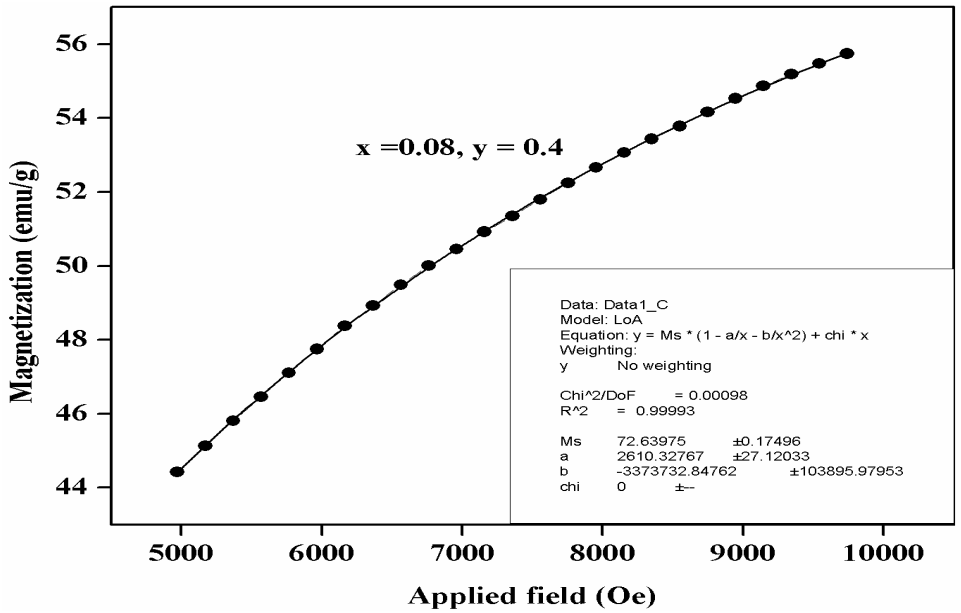

Figure 4e: The fitted curve of M_s at 300 K was obtained from the law of approach to saturation for $Co_{0.92}Tb_{0.08}Fe_{1.6}Cr_{0.4}O_4$ ferrite.

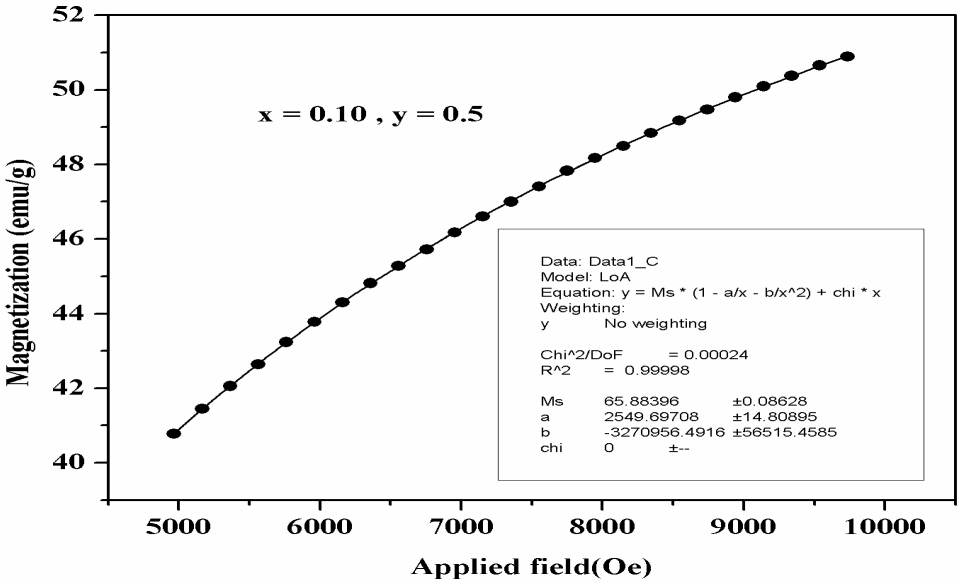

Figure 4f: The fitted curve of M_s at 300 K was obtained from the law of approach to saturation for $Co_{0.90}Tb_{0.10}Fe_{1.5}Cr_{0.5}O_4$ ferrite

Table 2
Saturation magnetization (M_s), Remanence (M_r) and Coercivity (H_c) for $Co_{1-x}Tb_xFe_{2-y}Cr_yO_4$ (x = 0.0-0.1, y=0.0-0.5) nano-ferrites

Composition	Ms (emu/g)	Mr (emu/g)	Hc (Oe)
x=0.00, y=0.0	62	13.38	425
x=0.02, y=0.1	61	10.96	397
x=0.04, y=0.2	59	10.11	398
x=0.06, y=0.3	58	8.12	365
x=0.08, y=0.4	56	9.10	399
x=0.10, y=0.5	51	8.29	409

3.4. Dielectric Properties

Ferrites are dipolar materials as they have Fe^{2+} cations in the minority Fe^{3+} cations in the majority. Dipoles of Fe^{3+}-Fe^{2+} align in the direction of the electric field. It can be seen from figure 5 that at a lower frequency, the dielectric constant (ε') decreases quickly. Still, it decreases gradually at the higher frequency region and becomes almost independent of frequency. In the literature, other researchers have reported a similar dielectric behavior

(D.R. Patil, 2009; N. Singh, 2011). In this research work, the movement of electrons between Fe^{3+} cations and Fe^{2+} cations and the movement of holes between Ni^{2+} cations and Ni^{3+} cations contributes to the local direction of electrons in the electric field, resulting in polarization. Koop's theory is helpful to interpret this fast decrement of dielectric constant at minimum frequency (Koops, 1951). On the basis of Koop's phenomenological theory dielectric structure having inhomogeneous medium consisting of two layers and this is also ascribed to the Maxwell- Wagner model (Jacob, Thankachan, Xavier, & Mohammed, 2013). This is evident from figure 5 that the dielectric constant is reduced by incorporating dopants (Tb^{3+}-Cr^{3+}).

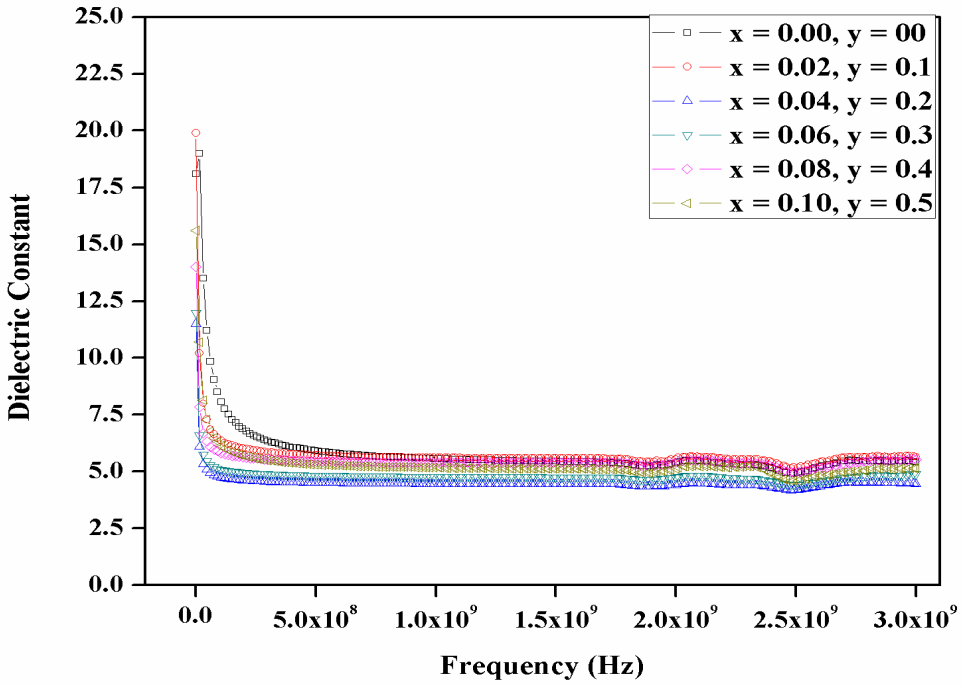

Figure 5: Dielectric constant (ε') vs frequency for $Co_{1-x}Tb_xFe_{2-y}Cr_yO_4$ (x = 0.0-0.1, y = 0.0- 0.5) ferrites

In ferrites, there are two losses, including magnetic loss and dielectric loss. Figures 6 and 7 indicate the dielectric loss (ε'') and tan loss of Tb-Cr doped cobalt ferrite. Figure 7 shows that dielectric tan loss decreases by increasing the number of dopants. The dielectric loss initially decreases rapidly and then increases slowly, and the last composition exhibits strange behavior. The variation in dielectric losses is because of the ion shifting. The loss peak is usually observed when the frequency of the external electric field becomes equal to the hopping frequency of the electron between Fe^{2+} and Fe^{3+} ions.

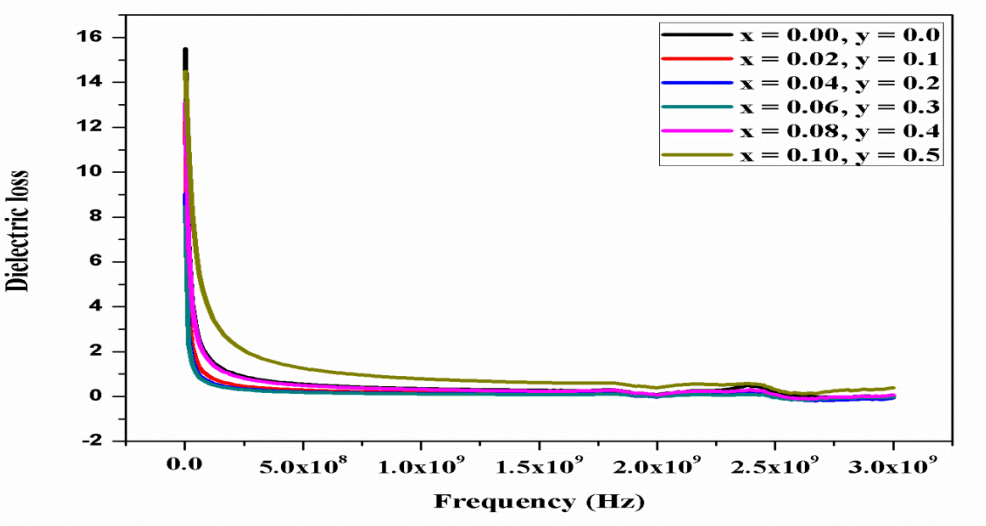

Figure 6: Dielectric loss (ε'') vs frequency for $Co_{1-x}Tb_xFe_{2-y}Cr_yO_4$ (x = 0.0-0.1, y = 0.0- 0.5) ferrites

The resonance phenomenon happens because of the matching of frequencies of external electric field and hopping frequency of transferring electrons. When dopants are incorporated in cobalt ferrite, it occupies the octahedral site, decreasing the number of cobalt and iron ions on that site. Due to this, electrical conduction decreases (Zhijian Penga, 2011). AC conductivity was calculated using the following equation:

$$\sigma_{ac} = 2\pi f \varepsilon' \varepsilon'' tan\delta \quad (2)$$

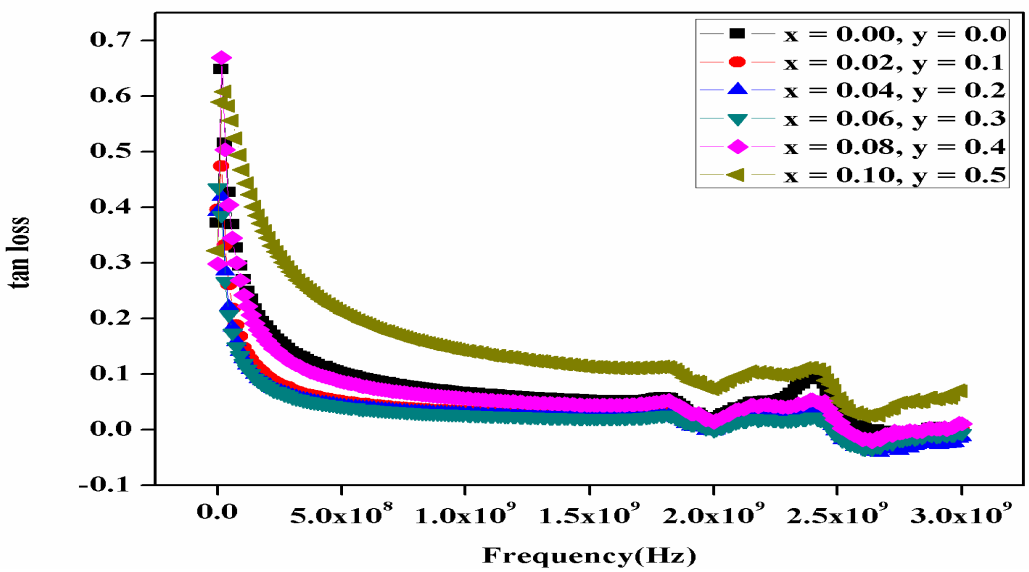

Figure 7: Tan loss vs frequency of $Co_{1-x}Tb_xFe_{2-y}Cr_yO_4$ (x=0.0-0.1,y=0.0-0.5) ferrites

Figure 8 shows that AC conductivity rises with the increase of doping contents of Tb^{3+} - Cr^{3+}. Figure 8 reveals that ac conductivity rise with the rise in frequency. This behavior can be explained using Maxwell Wagner's models and Koop's theory. Based on these models, ferrites are called conducting grains separated by a thin resistive layer called grain boundaries. In the lower frequency region, grain boundaries are more active and contribute to conduction. In higher frequency regions, conductive grains increase conduction and hoping conduction (Asif Iqbal et al., 2014). Peaking behavior is also observed beyond 1.5 GHz, which reveals the resonance phenomenon. The decrement in the AC conductivity with the increased dopants is ascribed to a decrease in the hoping frequency of electrons between Fe^{2+} and Fe^{3+}. The decrease in AC conductivity may be described by grain size. Since grain size declines for higher dopants concentration and hence grain boundaries become larger, AC conductivity declines.

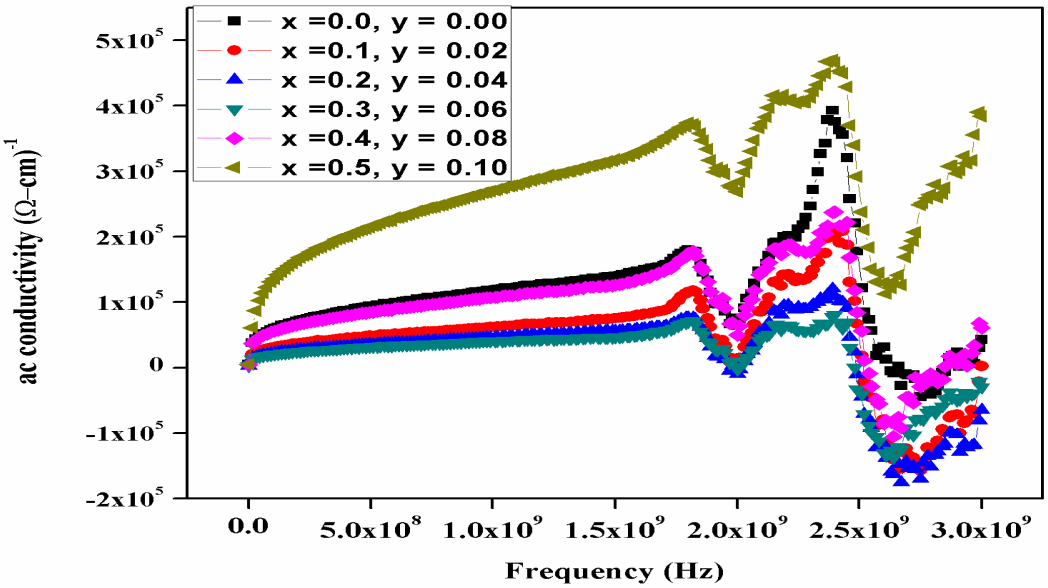

Figure 8: AC conductivity vs frequency for $Co_{1-x}Tb_xFe_{2-y}Cr_yO_4$ (x=0.0-0.1, y=0.0-0.5) ferrites

In ferrites, the conduction mechanism and relaxation behavior can be understood from the interpretation of the dielectric modulus. The real and imaginary parts of the dielectric modulus can be obtained using the following equations:

$$M' = \varepsilon' / (\varepsilon'^2 + \varepsilon''^2) \quad (3)$$

$$M'' = \varepsilon'' / (\varepsilon'^2 + \varepsilon''^2) \quad (4)$$

The nature of real (M') and imaginary (M'') parts of electric modulus as a function of applied field frequency is significant to knowing the relaxation mechanism (Asif Iqbal et al., 2014). Figure 9 and figure 10 indicate the real (M') and imaginary (M'') parts of the dielectric modulus as a function of applied frequency. M'' increases with the rise in the biasing oscillating applied electric field and reaches the highest value at some applied frequency called relaxation frequency. An oscillating frequency and applied field frequency become equal. According to these figures (9 &10), when the contents of dopants (Tb^{3+}-Cr^{3+}) increased highest peaks in M'' shifts towards the lower frequency region. This decrease in maxima peak with increased doping concentration for different compositions suggests the contribution of the grain boundary resistance (Pervaiz & Gul, 2014). These graphs show the missing relaxation phenomenon in these doped cobalt ferrites associated with the relaxation process (Pervaiz & Gul, 2014). This may be the reason for low loss, which makes these ferrites bad conducting and low dielectric loss to be used in an instrument that absorbs electromagnetic radiation (Asif Iqbal et al., 2014).

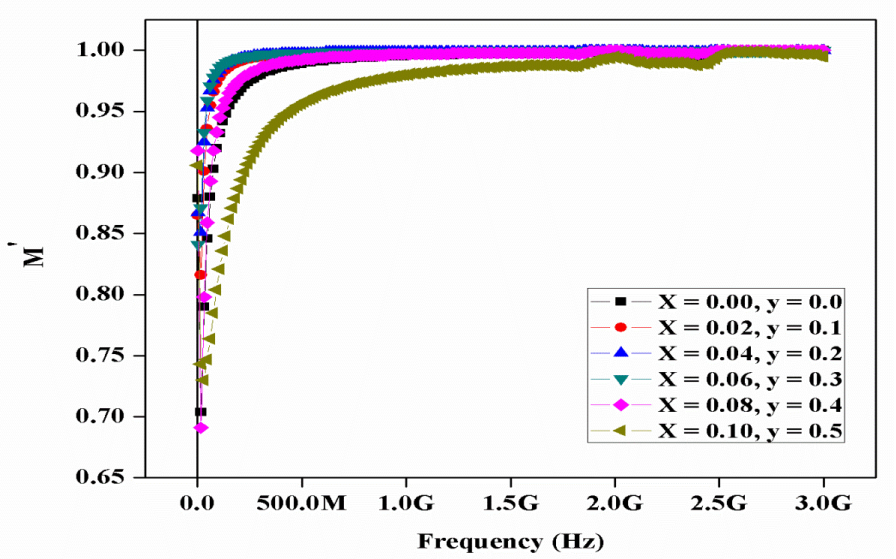

Figure 9: Real part of electric modulus vs frequency for $Co_{1-x}Tb_xFe_{2-y}Cr_yO_4$ (x=0.0-0.1 and y = 0.0- 0.5) ferrites

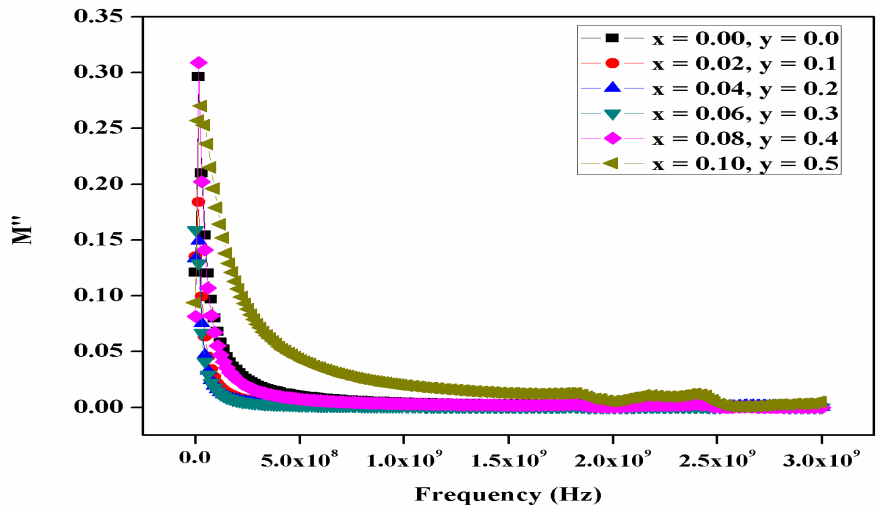

Figure 10: Imaginary part of electric modulus vs frequency for $Co_{1-x}Tb_xFe_{2-y}Cr_yO_4$ (x = 0.0-0.1 and y = 0.0- 0.5) ferrites

4. Conclusion

Tb-Cr substituted cobalt soft ferrites having the following compositions $Co_{1-x}Tb_xFe_{2-y}Cr_yO_4$ (x = 0.0-0.10, y = 0.0-0.5) were synthesized by solid-state reaction method. $CoFe_2O_4$ has a single-phase cubic spinel structure, and all other doped compositions exhibited traces of the ortho phase ($TbFeO_3$) and the cubic spinel phase. The structural and physical parameters depended strongly on the amount of dopants concentration. By increasing the dopants' contents following parameters were optimized as lattice constant (a, b, c), cell volume (V), and crystallite size (D). Magnetic parameters like M_s, M_r, and H_c were obtained from M-H loops. M_s was found in 51 emu/g -61 emu/g, and H_c lies in 364 Oe - 425 Oe. The H_c of prepared cobalt ferrites was found to be minimum, indicating that these materials can serve as potential candidates for high-density data storage devices applications. The polarization phenomenon was greatly influenced by increasing terbium and chromium concentration in cobalt ferrite. The dielectric constant and dielectric loss were found to decrease with the increase in dopants. The conduction phenomenon in these ferrites was impeded by introducing the Tb-Cr contents.

References

Ahmed, M. A., Afify, H. H., El Zawawia, I. K., & Azab, A. A. (2012). Novel structural and magnetic properties of Mg doped copper nanoferrites prepared by conventional and wet methods. *Journal of Magnetism and Magnetic Materials, 324*(14), 2199-2204. doi:http://dx.doi.org/10.1016/j.jmmm.2012.02.025

Asif Iqbal, M., Islam, M. U., Ali, I., khan, M. A., Sadiq, I., & Ali, I. (2014). High frequency dielectric properties of Eu+3-substituted Li–Mg ferrites synthesized by sol–gel auto-combustion method. *Journal of Alloys and Compounds, 586*(0), 404-410. doi:http://dx.doi.org/10.1016/j.jallcom.2013.10.066

B. Cheng, S. Q., H. Zhou, Z. Wang. (2006). Porous ZnAl 2 O 4 spinel nanorods doped with Eu 3 þ *synthesis and photoluminescence, Nanotechnology, 17*.

Batoo, K. M., Kumar, S., Lee, C. G., & Alimuddin. (2009). Finite size effect and influence of temperature on electrical properties of nanocrystalline Ni–Cd ferrites. *Current Applied Physics, 9*(5), 1072-1078. doi:http://dx.doi.org/10.1016/j.cap.2008.12.002

Bhandare, M., Jamadar, H., Pathan, A., Chougule, B., & Shaikh, A. (2011). Dielectric properties of Cu substituted Ni 0.5− x Zn 0.3 Mg 0.2 Fe 2 O 4 ferrites. *Journal of Alloys and Compounds, 509*(6), L113-L118.

D.R. Patil, B. K. C. (2009). *Mater. Chem. Phys, 117*, 1.

Dascalu, G., Popescu, T., Feder, M., & Caltun, O. F. (2013). Structural, electric and magnetic properties of CoFe1.8RE0.2O4 (RE=Dy, Gd, La) bulk materials. *Journal of Magnetism and Magnetic Materials, 333*(0), 69-74. doi:http://dx.doi.org/10.1016/j.jmmm.2012.12.048

Duan, H.-z., Zhou, F.-l., Cheng, X., Chen, G.-h., & Li, Q.-l. (2017). Preparation of hollow microspheres of Ce 3+ doped NiCo ferrite with high microwave absorbing performance. *Journal of Magnetism and Magnetic Materials, 424*, 467-471.

Farhadi, S., & Rashidi, N. (2010). Preparation and characterization of pure single-phase BiFeO3 nanoparticles through thermal decomposition of the heteronuclear Bi[Fe(CN)6]·5H2O complex. *Polyhedron, 29*(15), 2959-2965. doi:http://dx.doi.org/10.1016/j.poly.2010.08.019

Gadkari, A. B., Shinde, T. J., & Vasambekar, P. N. (2013). Influence of rare earth ion (Y3+) on the magnetic and dc electrical properties of high density nanocrystalline MgCd ferrites. *Materials Research Bulletin, 48*(2), 476-481. doi:http://dx.doi.org/10.1016/j.materresbull.2012.11.009

Grossinger, R. (1981). *Phys. Stat. Sol, 66(A)*.

Iqbal, M. J., Ahmad, Z., Meydan, T., & Nlebedim, I. C. (2012). Influence of Ni–Cr substitution on the magnetic and electric properties of magnesium ferrite nanomaterials. *Materials Research Bulletin, 47*(2), 344-351. doi:http://dx.doi.org/10.1016/j.materresbull.2011.11.011

Jacob, B. P., Thankachan, S., Xavier, S., & Mohammed, E. M. (2013). Effect of Tb3+ substitution on structural, electrical and magnetic properties of sol–gel synthesized nanocrystalline nickel ferrite. *Journal of Alloys and Compounds, 578*(0), 314-319. doi:http://dx.doi.org/10.1016/j.jallcom.2013.04.147

John Berchmans, L., Kalai Selvan, R., Selva Kumar, P. N., & Augustin, C. O. (2004). Structural and electrical properties of Ni1−xMgxFe2O4 synthesized by citrate gel process. *Journal of Magnetism and Magnetic Materials, 279*(1), 103-110. doi:http://dx.doi.org/10.1016/j.jmmm.2004.01.073

Kakade, S., Kambale, R., Kolekar, Y., & Ramana, C. (2016). Dielectric, electrical transport and magnetic properties of Er 3+ substituted nanocrystalline cobalt ferrite. *Journal of Physics and Chemistry of Solids, 98*, 20-27.

Kambale, R. C., Song, K. M., Won, C. J., Lee, K. D., & Hur, N. (2012). Magnetic and magnetostrictive behavior of Dy3+ doped CoFe2O4 single crystals grown by flux method. *Journal of Crystal Growth, 340*(1), 171-174. doi:http://dx.doi.org/10.1016/j.jcrysgro.2011.12.007

Khan, M. A., Islam, M. U., Ishaque, M., Rahman, I. Z., Genson, A., & Hampshire, S. (2009). Structural and physical properties of Ni–Tb–Fe–O system. *Materials Characterization, 60*(1), 73-78. doi:http://dx.doi.org/10.1016/j.matchar.2008.06.004

Khan, M. A., Javid ur Rehman, M., Mahmood, K., Ali, I., Niaz Akhtar, M., Murtaza, G., . . . Farooq Warsi, M. (2015). Impacts of Tb substitution at cobalt site on structural, morphological and magnetic properties of cobalt ferrites synthesized via double sintering method. *Ceramics International, 41*(2, Part A), 2286-2293. doi:http://dx.doi.org/10.1016/j.ceramint.2014.10.033

Koops, C. G. (1951). Koop's Phenomenological Theory. *Physica B: Condensed Matter, Review 83*, 1.

Kumar, G., Sharma, S., Kotnala, R. K., Shah, J., Shirsath, S. E., Batoo, K. M., & Singh, M. (2013). Electric, dielectric and ac electrical conductivity study of nanocrystalline cobalt substituted Mg–Mn ferrites synthesized via solution combustion technique. *Journal of Molecular Structure, 1051*(0), 336-344. doi:http://dx.doi.org/10.1016/j.molstruc.2013.08.019

Kumar, L., & Kar, M. (2012). Effect of La3+ substitution on the structural and magnetocrystalline anisotropy of nanocrystalline cobalt ferrite (CoFe2−xLaxO4). *Ceramics International, 38*(6), 4771-4782. doi:http://dx.doi.org/10.1016/j.ceramint.2012.02.065

Mahmood, A., Nadeem, M., Bashir, B., Shakir, I., Ashiq, M. N., Ishaq, M., . . . Warsi, M. F. (2013). Synthesis, characterization and studies of various structural, physical, magnetic, electrical and dielectric parameters for La1−xDyxNi1−yMnyO3 nanoparticles. *Journal of Magnetism and Magnetic Materials, 348*(0), 82-87. doi:http://dx.doi.org/10.1016/j.jmmm.2013.08.028

Mallapur, M. M., Shaikh, P. A., Kambale, R. C., Jamadar, H. V., Mahamuni, P. U., & Chougule, B. K. (2009). Structural and electrical properties of nanocrystalline cobalt substituted nickel zinc ferrite. *Journal of Alloys and Compounds, 479*(1–2), 797-802. doi:http://dx.doi.org/10.1016/j.jallcom.2009.01.142

Mukhtar, M. W., Irfan, M., Ahmad, I., Ali, I., Akhtar, M. N., Khan, M. A., . . . Ahmad, M. (2015). Synthesis and properties of Pr-substituted MgZn ferrites for core materials and high frequency applications. *Journal of Magnetism and Magnetic Materials, 381*(0), 173-178. doi:http://dx.doi.org/10.1016/j.jmmm.2014.12.072

N. Singh, A. A., S. Sanghi, Curr. 11 (2011) 783. (2011). *Appllied physics, 11*.

Ozkaya, T., Toprak, M. S., Baykal, A., Kavas, H., Köseoğlu, Y., & Aktaş, B. (2009). Synthesis of Fe3O4 nanoparticles at 100 °C and its magnetic characterization. *Journal of Alloys and Compounds, 472*(1–2), 18-23. doi:http://dx.doi.org/10.1016/j.jallcom.2008.04.101

Panneer Muthuselvam, I., & Bhowmik, R. N. (2010). Mechanical alloyed Ho3+ doping in CoFe2O4 spinel ferrite and understanding of magnetic nanodomains. *Journal of Magnetism and Magnetic Materials, 322*(7), 767-776. doi:http://dx.doi.org/10.1016/j.jmmm.2009.10.057

Patange, S. M., Shirsath, S. E., Lohar, K. S., Jadhav, S. S., Kulkarni, N., & Jadhav, K. M. (2011). Electrical and switching properties of NiAlxFe2−xO4 ferrites synthesized by chemical method. *Physica B: Condensed Matter, 406*(3), 663-668. doi:http://dx.doi.org/10.1016/j.physb.2010.11.081

Pervaiz, E., & Gul, I. H. (2014). High frequency AC response, DC resistivity and magnetic studies of holmium substituted Ni-ferrite: A novel electromagnetic material. *Journal of Magnetism and Magnetic Materials, 349*(0), 27-34. doi:http://dx.doi.org/10.1016/j.jmmm.2013.08.011

Ren, X., & Xu, G. (2014). Electromagnetic and microwave absorbing properties of NiCoZn-ferrites doped with La3+. *Journal of Magnetism and Magnetic Materials, 354*(0), 44-48. doi:http://dx.doi.org/10.1016/j.jmmm.2013.10.056

Rezlescu, N., Rezlescu, E., Pasnicu, C., & Craus, M. L. (1994). Comparison of the effects of TiO2-GeO2 and R2O3 substitutions in a high frequency nickel-zinc ferrite. *Journal of Magnetism and Magnetic Materials, 136*(3), 319-326. doi:http://dx.doi.org/10.1016/0304-8853(94)00309-2

Shirsath, S. E., Jadhav, S. S., Toksha, B., Patange, S., & Jadhav, K. (2011). Influence of Ce4+ ions on the structural and magnetic properties of NiFe2O4. *Journal of Applied Physics, 110*(1), 013914.

Sodaee, T., Ghasemi, A., Paimozd, E., Paesano Jr, A., & Morisako, A. (2013). The role of terbium cation substitution on the magnetic properties of cobalt ferrite nanoparticles. *Journal of Magnetism and Magnetic Materials, 330*(0), 169-173. doi:http://dx.doi.org/10.1016/j.jmmm.2012.10.050

Tahar, L. B., Artus, M., Ammar, S., Smiri, L. S., Herbst, F., Vaulay, M. J., . . . Fiévet, F. (2008). Magnetic properties of CoFe1.9RE0.1O4 nanoparticles (RE=La, Ce, Nd, Sm, Eu, Gd, Tb, Ho) prepared in polyol. *Journal of Magnetism and Magnetic Materials, 320*(23), 3242-3250. doi:http://dx.doi.org/10.1016/j.jmmm.2008.06.031

Wells, S., & Ramana, C. V. (2013). Effect of hafnium-incorporation on the microstructure and dielectric properties of cobalt ferrite ceramics. *Ceramics International, 39*(8), 9549-9556. doi:http://dx.doi.org/10.1016/j.ceramint.2013.05.073

Y. Y. Li, G. D. L. (1974). *The Physics of Ferrites, Beijing*.

Zhao, L., Cui, Y., Yang, H., Yu, L., Jin, W., & Feng, S. (2006). The magnetic properties of Ni0.7Mn0.3GdxFe2−xO4 ferrite. *Materials Letters, 60*(1), 104-108. doi:http://dx.doi.org/10.1016/j.matlet.2005.07.083

Zhijian Penga, n., Xiuli Fub,nn, Huilin Gea, Zhiqiang Fua, Chengbiao Wanga, Longhao Qic, Hezhuo Miaoc. (2011). Effect of Pr3 þdoping on magnetic and dielectric propertiesof Ni–Zn ferrites by ‘‘one-step synthesis’’. *Journal of Magnetism and Magnetic Materials 323 (2011) 2513–2518, 323* (05-05-2011), 6.